

# The imaging capabilities of the Frequency Agile Solar Radiotelescope

Stephen M. White<sup>a</sup>, Jeongwoo Lee<sup>b</sup>, Markus J. Aschwanden<sup>c</sup>, and Timothy S. Bastian<sup>d</sup>

<sup>a</sup>Dept. of Astronomy, Univ. of Maryland, College Park MD 20742, USA

<sup>b</sup>Dept. of Physics, New Jersey Inst. of Technology, Newark, NJ, USA

<sup>c</sup>Lockheed Martin, Palo Alto, CA, USA

<sup>d</sup>NRAO, Charlottesville, VA, USA

## ABSTRACT

The Frequency Agile Solar Radiotelescope (FASR) will observe the Sun over a wide range of radio frequencies and make high spatial resolution images at many frequencies nearly simultaneously. FASR will need to be able to observe both the very bright, usually compact emission from solar flares as well as much fainter fluctuations in the solar chromosphere across a broad range of spatial scales (from 1 arcsec to 1 degree) at high time resolution, and these constraints impose severe requirements on telescope design. We discuss the problem of imaging the Sun at radio wavelengths and present simulations of imaging the thermal free-free emission from the Sun's atmosphere using models based on EUV data.

**Keywords:** Radio telescopes, Solar radio astronomy

## 1. INTRODUCTION

The *Frequency Agile Solar Radiotelescope* (FASR) will be a solar-dedicated radio interferometric array that will be optimized to carry out imaging spectroscopy of the Sun, i.e., to produce high-quality, high spatial resolution images of the Sun simultaneously at a wide range of frequencies. FASR will perform coronal magnetography, detect and map nonthermal populations of electrons from the ground, and identify and track drivers of space weather. FASR has been highlighted by a number of NRC panels as an important resource for solar physics at the next solar maximum, and detailed planning for the project has commenced.

An important aspect of FASR is that it will not only, or even primarily, serve the solar radio astronomy community: it will serve a large user base comprising solar, solar-terrestrial, and space physicists. All FASR data will be made freely available. Instead of placing the burden of data calibration and reduction on the user, FASR data processing will be pipelined and the data will be made available as fully calibrated, optimally-deconvolved maps. FASR will “mainstream” the use of solar radio observations by the wider community, much as the Solar and Heliospheric Observatory (SOHO) and the Transition Region and Coronal Explorer (TRACE) satellites have mainstreamed the use of solar EUV data, and the *Yohkoh* satellite has mainstreamed the use of solar soft and hard X-ray imaging data. FASR will carry out dual roles, serving both as a basic research instrument and as a source of basic synoptic data that can be used to forecast solar conditions and space weather and geophysical disturbances. Hence FASR will provide a direct societal benefit.

A great deal of work has been done over several decades to characterize and understand solar radio emission processes and phenomena. The science to be done with FASR has been extrapolated from this experience, but FASR is such an advance over current instrumentation (in frequency coverage, image quality, spatial resolution, and sensitivity), that a true understanding of what it is capable of requires complex, three-dimensional source model simulations. These are important for refining such things as the array configuration, antenna number and antenna size. But they are also a critical

---

Further author information: (Send correspondence to S. White)

SMW: E-mail: white@astro.umd.edu

JWL: E-mail: lee@njit.edu, Address: Dept. of Physics, NJIT, 323 King Blvd, Newark NJ 07102-1982

MJA: E-mail: aschwanden@lmsal.com, Address: Lockheed Martin, Advanced Technology Center, Solar and Astrophysics Lab., Dept. L9-41, Bldg 252, 3251 Hanover St, Palo Alto CA 94301

TSB: E-mail: tbastian@nrao.edu, Address: NRAO, 520 Edgemont Rd, Charlottesville, VA 22903-2475

means to understand observing strategies, calibration strategies, and image processing algorithms that will be necessary to maximize the usefulness and science return of the instrument. The models will be constructed by assembling space and ground-based information necessary to create one or more realistic three-dimensional active region and coronal mass ejection (CME) models, with the requisite spatial resolution ( 1 arcsec) and with appropriate complexity to test the ideas we have for measuring physical parameters of the solar atmosphere with FASR. The radio emission from the 3-D models will be calculated at a range of frequencies, viewed from different directions, sampled with the expected array configuration, and the resulting image cubes (in dual polarization) will be inverted and compared to the model to assess the precision of extracting the physical parameters. A flaring loop model will also be generated, with realistic distribution of particles and possibly also the appropriate time-dependent behavior. These models will guide the observing, calibration, and image processing strategies to be used by FASR. In this paper we present some early steps to this goal, using EUV images from the Extreme-ultraviolet Imaging Telescope (EIT) on SOHO to generate a quiet-Sun model radiating by free-free emission alone, processing this through a model array and comparing with actual images. The next section first provides a brief overview of the FASR project.

## 2. FASR OVERVIEW

The specifications for the Frequency Agile Solar Radiotelescope, as driven by science requirements, are shown in Table 1. While the specification in each category (frequency range, frequency resolution, time resolution, angular resolution, field of view) may seem relatively modest, it is the *combination* of characteristics that makes FASR such an advance over existing instruments.<sup>1</sup> The main characteristics that the instrument must have are:

- *Excellent Snapshot Imaging:* The Sun must be imaged with high dynamic range, fidelity, and angular resolution, with good sensitivity to both compact and extended sources of emission, *instantaneously*. A dynamic range  $\gtrsim 1000$ : 1 and an angular resolution of  $\approx 1''$  at a frequency of 20 GHz are considered reasonable goals.
- *Broadband spectroscopy:* Spectral coverage over a frequency range of 0.1-20 GHz is required to cover the scientifically relevant range of heights and phenomena of the solar atmosphere. Continuous frequency coverage over this range is needed to obtain high-resolution spectral diagnostics. Coverage up to 30 GHz is desirable for particle acceleration diagnostics.
- *Polarimetry:* Dual polarization observations are required for coronal magnetography and particle acceleration diagnostics. The correlations required to form all four Stokes parameters are desirable, but not necessarily over the entire frequency range or at all times.
- *High time resolution:* Spectra must be acquired at a rate sufficient to follow spectral variations during solar flares. At centimeter wavelengths a full spectrum (2-20 GHz) must be obtained in  $\lesssim 1$  sec. At decimeter wavelengths, the requirement is more demanding:  $\lesssim 0.1$  sec on a routine basis, with even higher rates over restricted bandwidths as required.
- *Large field of view:* Imaging over the full solar disk ( $\frac{1}{2}^\circ$ ) or larger is desired over a significant portion of the spectral range of the instrument, for mapping coronal mass ejections and maximizing the science return.
- *Absolute positional accuracy:* FASR should match space and optical ground-based instrument resolutions of order 1 arcsec. Quantitative cross-comparisons of FASR observations with those in other wavelength regimes will require precise knowledge of absolute source positions.
- *Easy access by the scientific community:* As an operational requirement, the instrument must not place the burden of data reduction on the user. Most of the calibration and data reduction should be performed on-site with a data pipeline, and a wide variety of data products should be made available for immediate use.

Although FASR was conceived entirely separately from other radiotelescope projects now being considered, it has obvious similarities to the Allen Telescope Array (ATA) and to the Low Frequency Array (LOFAR). LOFAR can be considered complementary to FASR, in that its frequency range will extend below FASR's frequency range. LOFAR will carry out interesting and important solar and heliospheric science that is complementary to the key science of FASR.<sup>2</sup> The

**Table 1. FASR Specifications**

Number of antennas	$\sim 100$	Frequency range	0.1–30 GHz (core: 0.5–18 GHz)
Number of baselines	$\sim 5000$	Frequency resolution	$\sim 1\%$ , 2–30 GHz
Antenna size	D = 2 - 6 m		$\sim 0.1\%$ , 0.1–2 GHz
Angular resolution	$\approx (20/v_9)$ arcsec	Time resolution	$\lesssim 0.1$ sec, 2–30 GHz
Field of view	$\approx 1030/(v_9 D)$ arcmin		$\lesssim 0.01$ sec, 0.1–2 GHz
Polarization	Full	Number IFs pairs	4 - 8

ATA has a similar frequency range of 0.5–11.5 GHz, and will employ several hundred antennas to obtain excellent snapshot image quality. FASR shares many of the key technology challenges of ATA. ATA differs from FASR in having shorter baselines, a smaller frequency range, and weaker pointing constraints, but more severe spectral processing requirements and many more antennas.

### 3. RADIO IMAGING OF THE SUN

The imaging process has always been a drawback for radio astronomy, in the sense that, unlike conventional optical telescopes, interferometers do not image directly: to exploit the full power of an interferometer one usually has to invert the measured visibilities, remove bad data, and deconvolve for the point response of the telescope, and the practical difficulties that attend these steps have led to the term “black belt radio astronomer”, a term that may be viewed as an honorific amongst radio astronomers but one that is off-putting to the casual user from other wavelength ranges. Considerable effort will be put into avoiding this perception for FASR data, in order that they should be accessible to as wide a community as possible. To this end, we anticipate that most users will only ever deal with fully calibrated

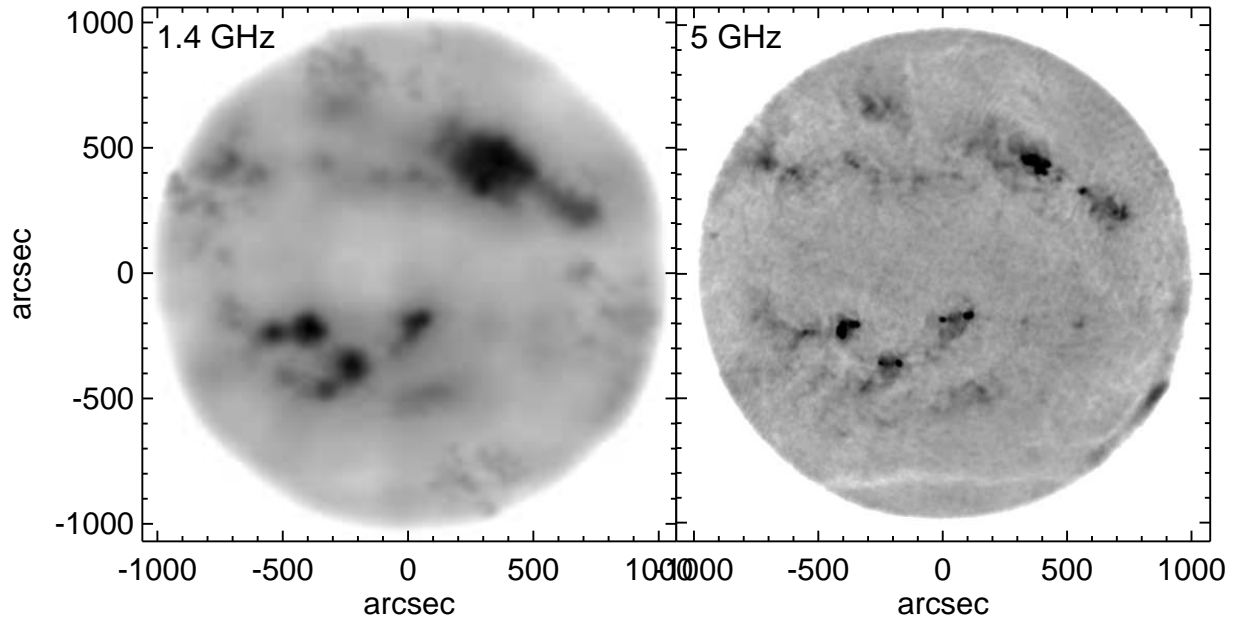


**Figure 1.** Full disk radio images of the Sun at (left) 1.4 GHz and (right) 4.6 GHz made with the Very Large Array in “D” configuration on 1999 April 11. In this configuration the full disk fits into the primary beam of the VLA antennas at 1.4 GHz, but the visibilities do not adequately sample the full disk spatial scales, so a disk is supplied as a default model in deconvolution. The restoring beam size at 1.4 GHz is  $40''$ . At 4.6 GHz the primary beam is just  $10'$ : the image shown here is made by mosaicking techniques in which 26 different fields across the Sun are observed and deconvolved with a disk supplied as the default model. The restoring beam size is  $12''$ . The greyscale is a logarithmic representation of the intensity from 4000 K to  $1.9 \times 10^6$  K at 1.4 GHz and from 4000 K to  $9 \times 10^5$  K at 4.6 GHz.

and deconvolved FASR images; the unit most useful to users is probably that of brightness temperature, since it actually represents the local temperature in any optically thick radio source.

The need to supply processed images on demand imposes a burden on the pipeline processing tasks used for the purpose. Here we can take advantage of the fact that we know a lot about the appearance of the Sun at radio wavelengths, and can make use of this knowledge to simplify the imaging process. One important feature is that the size of the radio source is well understood, and except at low frequencies we need only image to a radius of about  $2400''$  to cover virtually all solar phenomena that FASR will be able to detect. However, the fact that the Sun's radio emission fills such a large area on the sky poses a problem for algorithms such as CLEAN, which is really best suited to deconvolving bright sources that have emission in a small number of pixels. Over most of its frequency range FASR will have the entire solar disk within its field of view (FWHM of a dish of diameter  $D$  m at frequency  $f$  GHz is  $1030'/Df$ ), but it will not sample the very large spatial scales needed to reconstruct completely the solar brightness at all frequencies. The minimum projected spacing  $d$  between antennas determines the longest fringe spacing (the separation of peaks in the Fourier pattern on the sky) in the data, being  $1030'/df$ , with  $d$  in meters and  $f$  in GHz: this needs to be at least  $100'$  to fit the solar disk into a Fourier lobe, and hence at e.g., 10 GHz, one requires a minimum spacing of order 1 m which is smaller than planned dish sizes. Thus at high frequencies FASR, as an interferometer, will not be sensitive to the total solar disk flux (it may be possible to measure this quantity independently by a small single dish).

This is not the disadvantage that it might first seem to be because we have considerable experience in restoring data that do not fully sample the solar disk: Figure 1 shows radio images of the Sun from the Very Large Array at two different frequencies (1.4 and 4.6 GHz), neither of which fully samples the larger spatial scales of solar radio emission. These images have both been produced using a flat disk as a default model for maximum-entropy deconvolution. Pioneers in handling radio data that partially sample the solar disk have been the Nobeyama Radio Heliograph (NoRH) group.<sup>3,4</sup> NoRH consists of 84 small (80 cm diameter) dishes operating at 17 and 34 GHz. The dishes are too small to detect sources other than the Sun with uncooled receivers at these frequencies, so they use the Sun itself as a calibration source: at these frequencies the solar disk dominates the quiet-Sun flux and a solar-disk model of a 10000 K source of appropriate radius, in combination with designed redundancy in the array, works well for calibrating the data. In imaging NoRH data, one generally subtracts the solar disk from the raw data before proceeding, in order to avoid having to deconvolve a large flat disk, and this works well in practice. It is intended that FASR will be able to detect astrometric calibrators with the advantage of its large bandwidth, and position calibration can then be carried out in conventional fashion. At most frequencies FASR imaging will probably proceed only after first subtracting a frequency-dependent model disk, whose radius and brightness will be known a priori, from the data. The model disk can then be restored after deconvolution of the other emission features.

#### 4. FREE-FREE MODEL OF THE RADIO SUN

Figure 1 shows a number of features important for routine mapping of the Sun by FASR: the brightest features in a quiet-Sun radio image are usually at coronal temperatures of several million K, and the disk varies in brightness temperature from  $10^6$  K at low frequencies, where the solar atmosphere is optically thick in the corona due to thermal free-free (bremsstrahlung), to  $10^4$  K at high frequencies ( $\sim 20$  GHz), where the corona is optically thin and one sees down to the solar chromosphere. At 1 GHz the quiet-Sun disk temperature is about  $10^5$  K, while at 5 GHz it is 30000 K. Despite the fact that the optically thick layer one sees down to in the atmosphere becomes cooler and cooler as frequency rises, the corresponding solar disk contribution to the radio emission becomes an increasingly prominent feature at higher frequencies because the brightness temperature of the optically thin coronal features decreases as  $f^{-2}$ , which is much faster than the rate of decrease of the apparent disk temperature.

In the remainder of this paper we carry out some data simulations for the date shown in Figure 1, 1999 April 11. We simulate primarily the bremsstrahlung component of the atmosphere: the brightest features in the 4.6 GHz radio image are gyroresonance sources that are optically thick in the corona because of the strong magnetic fields over active regions. This gyroresonance emission will be only briefly discussed here.

To derive a radio model incorporating the free-free emission from the solar atmosphere, we use coronal temperatures and emission measures derived from EUV images from the Extreme-ultraviolet Imaging Telescope (EIT) on the SOHO spacecraft. Here we use Fe IX/X 171 Å and Fe XII 195 Å EIT images with a pixel size (from Earth) of  $2.602''$ . Temperature and emission measure maps are derived using standard EIT procedures. The results do not completely characterize

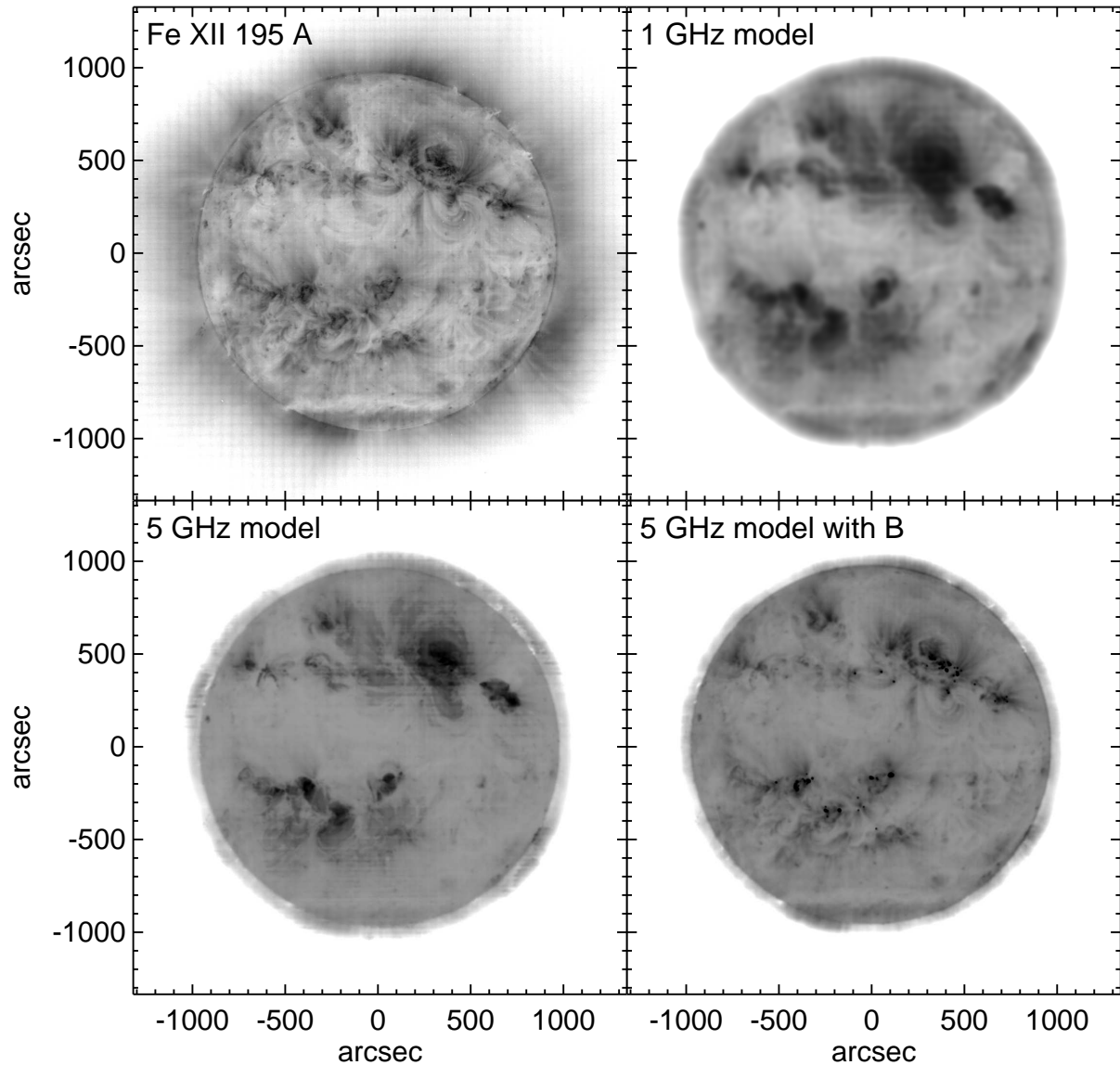


**Figure 2.** The SOHO/EIT Fe XII 195 Å image (upper left) on 1999 April 11 used to determine the model for the simulations, the 1 GHz model (upper right) resulting from a free-free calculation and convolved with a 30'' beam, the 5 GHz free-free model (lower left) resulting from the EIT data and convolved with an 8'' beam, and the 5 GHz model including both free-free contributions and gyroresonance sources determined using a SOHO/MDI line-of-sight magnetogram. The temperature and emission measure derived from the EIT data are used to derive bremsstrahlung optical depths ( $\propto f^{-2}$ ) and then brightness temperatures. A chromospheric contribution is added to the coronal emission, and the model as shown here is convolved with a gaussian of size appropriate to the observation for comparison with the model FASR images. The images are shown with the grey colors scaled logarithmically.

the solar atmosphere by any means: the pair of EIT images used is only sensitive to cool coronal material and is not even comprehensive for the material to which EIT is sensitive,<sup>5,6</sup> but they serve as an appropriate starting point. The EUV data also do not incorporate the contribution of the solar chromosphere to the radio emission. We add this contribution separately, following the measurements of Zirin et al.<sup>7</sup>

The procedure is to rotate the EIT images to a common time, determine the temperature and emission measure maps (corrected for the abundance of Fe<sup>8</sup>), calculate the (frequency-dependent) optical depth due to bremsstrahlung in each

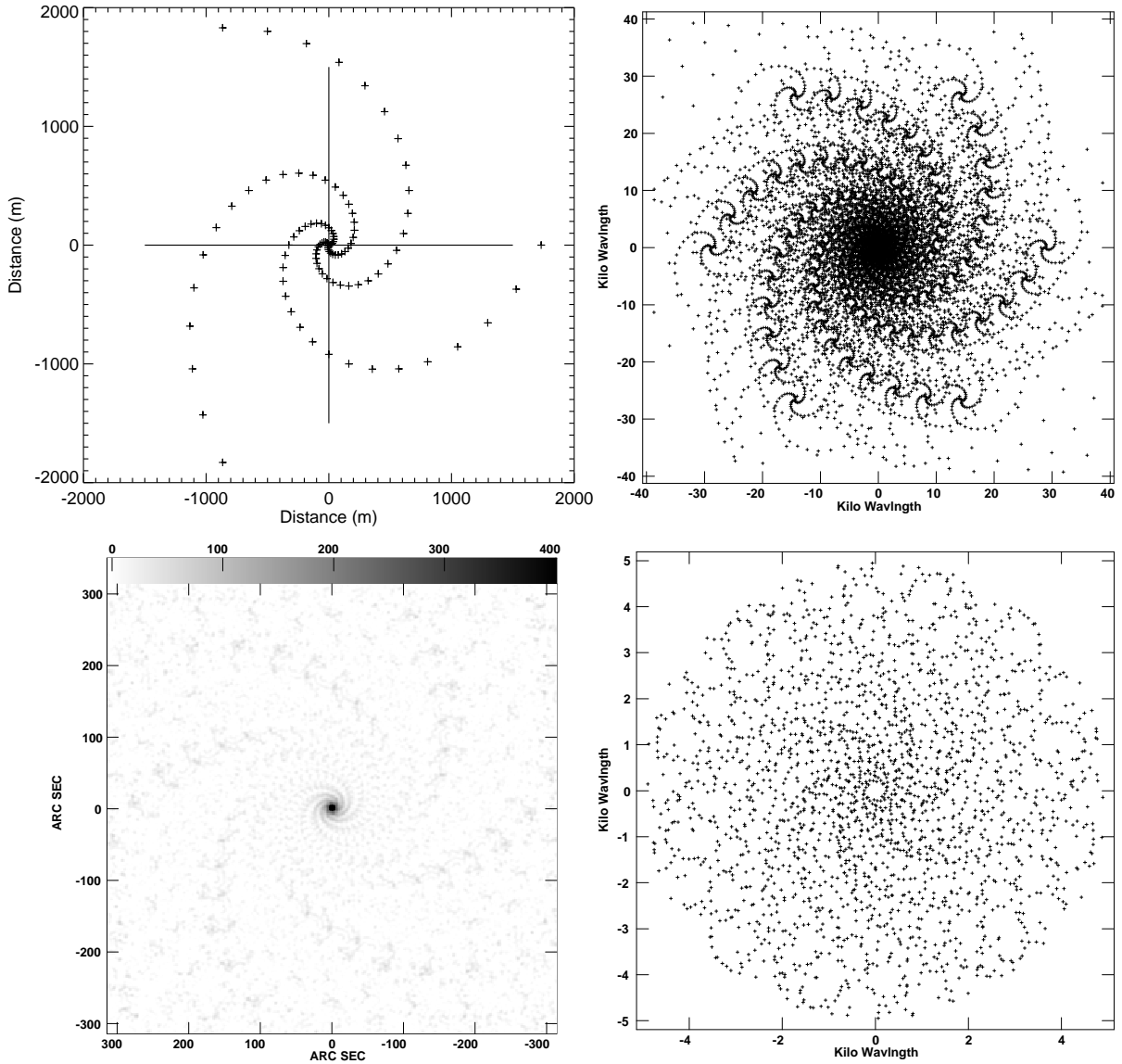


**Figure 3.** The snapshot and beam resulting from a candidate log-spiral configuration of 99 antennas. In this case the minimum spacing is 10m. The panels show (a) top left, the antenna layout, with 33 antennas on each arm and a wrap of 1 turn per arm; (b) top right, the  $u, v$  configuration resulting from this configuration at 5 GHz at transit on 1999 April 11; (c) bottom left, the beam pattern resulting from this configuration, with the greyscale showing the range from -3% to 40% of the beam peak: the largest negative value in the beam is -3%; and (d) bottom right, details of the inner region ( $< 5$  kilo $\lambda$ ) of the  $u, v$  distribution which is saturated in the panel above.

pixel using standard formulae,<sup>9</sup> determine the corresponding brightness temperature ( $T_b = T_e(1 - e^{-\tau})$ ) and then convert to radio flux. The chromospheric contribution is then added for pixels on the solar disk. Emission above the limb also has to be suppressed in the model, because the EIT images suggest more material there than is actually present due to contamination by other lines and off-limb calibration. The EIT images also show a grid pattern that is instrumental; it is partially removed by the calibration procedure, and we have not attempted to remove the residual features.

The original EIT image and typical resulting model radio images (here for 1 and 5 GHz) are shown in Figure 2. The 1 GHz radio model has been convolved with a  $30''$  beam and the 5 GHz model with an  $8''$  beam for comparison with the final maps. As required, the solar disk is a prominent feature of the radio model despite being largely absent from

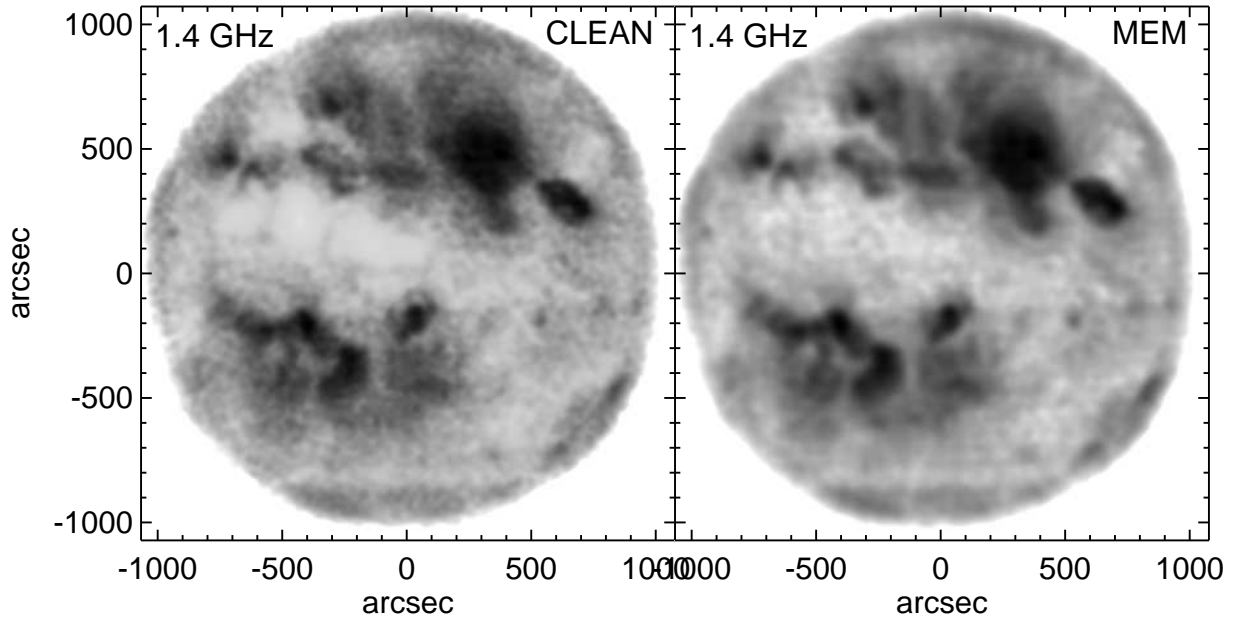


**Figure 4.** 1.0 GHz model images processed through the test FASR configuration (Fig. 3). The panel on the left is a CLEAN image (disk subtracted from visibilities, residuals CLEANed, then disk restored to the subsequent image) while that on the right is a maximum-entropy deconvolution using the same disk as a default model. The restoring beam size is  $30''$  (weighting intermediate between natural and uniform). These images may be compared with the observed image (Fig. 1) and the model image (Fig. 2). Note that the 1.4 GHz image in Fig. 1 is the result of a 12 hour synthesis observation by the VLA, whereas the images shown here are the result of snapshot observations. The display is logarithmic from 4000 to  $1.9 \times 10^6$  K.

the Fe XII image: in the radio image it is due to the chromosphere, which is absent from the EUV coronal images. The brightest features in the radio model are exactly those that are brightest in the EIT image, since they are the densest regions in the corona and hence have the largest optical depths at radio wavelengths. Note however that some features are underrepresented in the radio model: the filament channel around the south pole that is prominent in the Fe XII image is barely discernible in the radio image, because it lies in a region of weak emission in the Fe XII image that produces only a small coronal brightness temperature contribution to the radio model. This contribution is much smaller than the solar disk contribution from the chromosphere, and the contrast of the filament channel does not show up in the model against this brighter background. The actual observation (Fig. 1) does show the filament channel as a prominent feature that we attribute to a chromospheric signature that is not included in the models.

To show the effects of including magnetic fields in the calculation of the radio models, Fig. 2 also presents a 5 GHz model in which gyroresonance sources are added using the simple approach of assuming that the corona is optically thick at the temperature derived from the EUV data if the magnetic field in that pixel exceeds the value required to match the third harmonic of the local gyrofrequency. The magnetic field is estimated from a SOHO/MDI line-of-sight magnetogram obtained at 19 UT (essentially the same time as the EUV data). The result is a number of bright compact sources at brightness temperatures in excess of  $10^6$  K that are much brighter than anything in the free-free model. Many of these sources can be seen to be present in the VLA image in Fig. 1.

## 5. SIMULATED IMAGES

For imaging simulations here we use an array consisting of 99 antennas arranged on 3 essentially log-spiral arms each making a full  $360^\circ$  turn. The outer antennas are approximately 1700 m from the array center, and the maximum baseline length is about 3 km. The antenna size is 6 m and the minimum antenna separation is 10 m. The array is shown in Figure 3 together with the snapshot  $u, v$  distribution and the resulting snapshot beam pattern. The model data described are converted into a model observation using the NRAO AIPS task UVCON.<sup>10</sup> This array is just an example of a possible

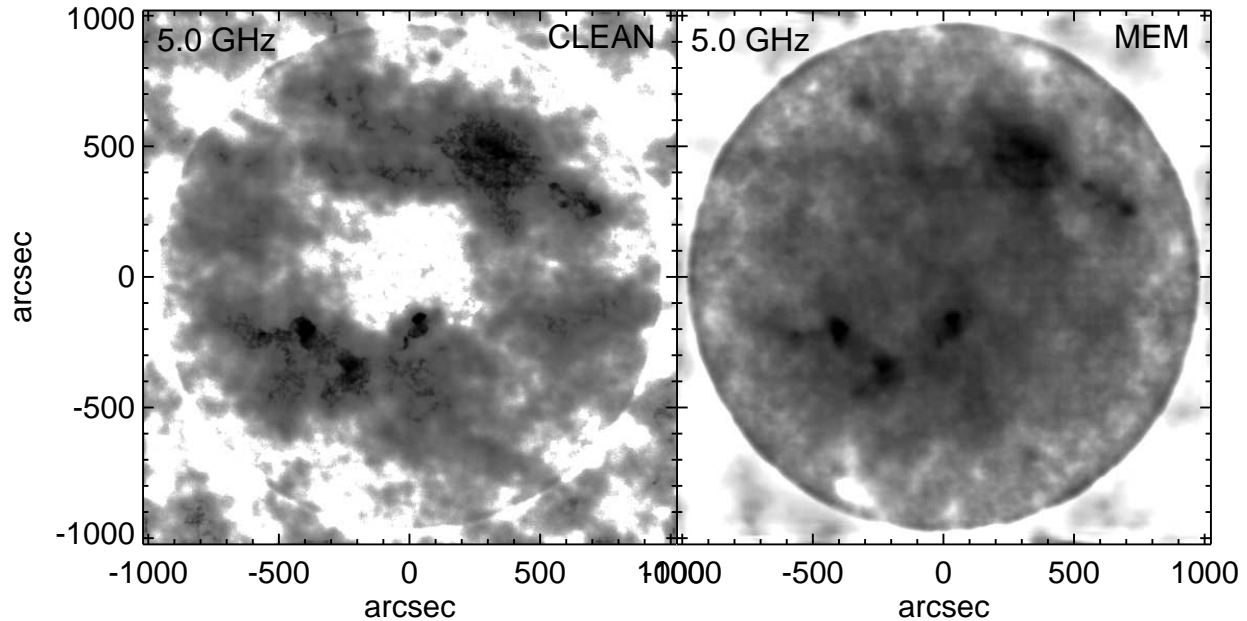


**Figure 5.** 5.0 GHz model images processed through the test FASR configuration consisting of 99 6-m dishes. The panel on the left is a CLEAN image (disk subtracted from visibilities, residuals CLEANed, then disk restored to the subsequent image) while that on the right is a maximum-entropy deconvolution using the same disk as a default model. The restoring beam size is  $8''$ . These images may be compared with the observed image (Fig.1) and the model image (Fig. 2).

configuration that FASR might use: log-spiral arrays are one of several configurations being considered for large arrays such as the Atacama Large Millimeter Array.<sup>11,12</sup> The visibilities are weighted to produce a beam intermediate between pure natural and pure uniform weighting; the resulting snapshot beam for this array has a maximum negative of just 3% of the beam maximum, but it does have a significant widespread spiral pattern of positive response at a low level that can spread flux over a wide area from the many pixels filled by solar emission.

The results of analyzing the model data at 1 GHz are shown in Figure 4, which can be compared with the starting model in Fig. 2 and the actual VLA 1.4 GHz observation in Fig. 1. Two deconvolution techniques are compared here. One is the “CLEAN” approach,<sup>13</sup> but with the disk component subtracted from the visibility data first and then restored in the image plane after deconvolution to avoid having to clean the flux in all the disk pixels due to this component. The second technique is to make dirty maps and then deconvolve them using the maximum entropy method<sup>14</sup> using the disk component as a default image. In this method the results can depend on whether or not the algorithm is forced to achieve a specific total flux. The minimum 10 m baseline does sample the full disk flux at 1 GHz, so the disk flux is reconstructed well no matter what the technique.

The two deconvolved images in Fig. 4 are essentially identical: the peaks in the difference image are typically less than 0.25% of the maximum, and appear to be dominated by small features typical of CLEAN images in which many clean components are required, leading to low-level instabilities. As noted above, the beam shown in Fig. 3 does have significant low-level response that spreads flux in the dirty map well outside the solar disk, and even after subtracting the disk it takes many clean components to clean the image well: even at the relatively low resolution of this image the solar disk contains over 4000 resolution elements and each of them contains flux.

The corresponding results at 5 GHz are shown in Figure 5. Here the frequency is too high for the array of 6 m dishes satisfactorily to sample the full solar disk, so in the maximum entropy approach one must specify the final total flux; if this is not done too little flux is recovered. In this case neither deconvolution does as well as in the 1 GHz models. The maximum entropy image appears to be a cosmetically satisfactory representation of the input model, but in detail it does not match the model well, and the 5 GHz CLEAN image is surprisingly poor. We suspect that a combination of reasons is responsible for this result. At this frequency the solar disk contains 60000 resolution elements, while only 9000 quantities

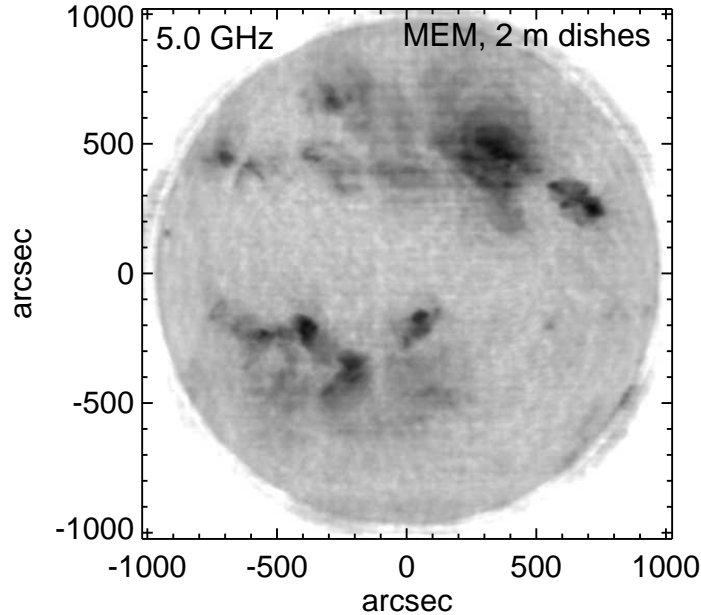


**Figure 6.** The 5.0 GHz model image processed through a test FASR configuration consisting of 99 2-m dishes with a minimum spacing of 3 m. The observation is for 30 minutes immediately following transit. The image is a maximum-entropy deconvolution using a flat disk as a default model. The restoring beam size is  $8''$ . This image may be compared with the observed image (Fig.1) and the model image (Fig. 2).

are measured by the observation (4500 baselines, each a complex number), so in principle the data do not contain enough information to reconstruct fully the model. Further, unlike the VLA, whose shortest baseline is about 40 m and therefore completely resolves out the solar disk scale at this frequency, the 10 m minimum antenna spacing of this test array means that the disk is present in the data but inadequately sampled.

For this reason, the current plan for FASR calls for an array of smaller dishes operating at frequencies above 3 GHz. We have simulated the imaging problem using the same 5 GHz free-free model observed by an array of 99 2-m dishes having a minimum spacing of 3 m and a realistic solar-dominated system temperature. In addition, we simulate the result of a 30-minute observation which helps to fill in the  $u, v$  plane somewhat. The result is shown in Figure 6 using MEM deconvolution with a default disk (CLEAN is less efficient than MEM because of the number of pixels required to cover the solar disk at the appropriate resolution). The deconvolution has not been optimized and we believe that this affects the restoration of the low surface brightness emission, but the brighter coronal free-free emission is recovered extremely well. When the brighter gyroresonant sources are also included, MEM deconvolution does not work as well: this is a well-known effect whose solution is to CLEAN and subtract the bright compact sources from the data before using MEM deconvolution on the remaining emission.

## 6. CONCLUSION

These results give an impression of the considerations that must be taken into account in designing FASR such that it can achieve its scientific goals. Here we have highlighted probably the most difficult issue for FASR imaging, namely the problem of dealing with emission from both large and small spatial scales over a wide frequency range. The need to obtain short-spacing data at high frequencies is emphasized by Fig. 5, and this drives FASR to include smaller dishes for the higher frequencies. In addition, observing strategies can ameliorate the lack of short spacings even with the 6 m antennas: it is well established that mosaicking observations with an interferometer (observations of fields of view that overlap by half a primary beam width) contain information on spatial scales corresponding to about half the shortest spacing.<sup>15-17</sup> This technique is used to create the 4.6 GHz VLA image of the Sun from 26 overlapping fields shown in Fig. 1. The combination of interferometer data with single dish measurements of the total power from the Sun will also

help to sample the large spatial scales,<sup>18</sup> and frequency-synthesis<sup>19,20</sup> may also help to fill in the snapshot  $u, v$  distribution for broadband sources. Nonetheless, Figs. 4 and 6 show the imaging power that FASR will deliver.

Additional simulations of a range of science issues (coronal magnetography, flare science, coronal mass ejections) will also be carried out in order to guide design decisions for the array. With the combination of images at many frequencies, each probing different depths in the solar atmosphere because of the frequency dependence of both free-free and gyroresonance opacity, and information from the two circular polarizations, FASR observations contain a great deal of information on the three-dimensional structure of the solar atmosphere (temperature  $T_e$ , density  $n_e$  and magnetic field strength  $B$ ). Considerable effort is needed before we can understand how much of the three-dimensional structure can be retrieved by “inversion” of the radio spectrum in each pixel.

## ACKNOWLEDGMENTS

This research was supported by NSF grants ATM 99-90809 and AST 01-38317, and NASA grants NAG 5-8192 and NAG 5-10175.

## REFERENCES

1. T. S. Bastian, “The frequency agile solar radiotelescope,” in *SPIE Proceedings: Innovative Telescopes and Instrumentation for Solar Astrophysics*, S. L. Keil and S. V. Avakyan, eds., SPIE, 2002. in press.
2. S. M. White, N. E. Kassim, and W. C. Erickson, “Solar astronomy with the LOw Frequency ARray (LOFAR) radiotelescope,” in *SPIE Proceedings: Innovative Telescopes and Instrumentation for Solar Astrophysics*, S. L. Keil and S. V. Avakyan, eds., SPIE, 2002. in press.
3. H. Nakajima, M. Nishio, S. Enome, K. Shibasaki, T. Takano, Y. Hanaoka, C. Torii, H. Sekiguchi, and 9 others, “The Nobeyama RadioHeliograph,” *Proc. IEEE* **82**, p. 705, 1994.
4. H. Koshiishi, S. Enome, H. Nakajima, K. Shibasaki, M. Nishio, T. Takano, Y. Hanaoka, C. Torii, H. Sekiguchi, S. Kawashima, T. Bushimata, N. Shinohara, Y. Irimajiri, and Y. Shiomi, “Evaluation of the imaging performance of the Nobeyama RadioHeliograph,” *Publ. Astron. Soc. Japan* **46**, p. L33, 1994.
5. J. Zhang, S. M. White, and M. R. Kundu, “Two-temperature-component modelling of the corona based on SOHO/EIT observations,” *EOS* **79(17)**, p. S290, 1998.
6. J. W. Cook, J. S. Newmark, and J. D. Moses, “Coronal Thermal Structure from a Differential Emission Measure Map of the Sun,” in *8th SOHO Workshop: Plasma Dynamics and Diagnostics in the Solar Transition Region and Corona*, **8**, p. 241, ESA Special Publication 46, 1999.
7. H. Zirin, B. M. Baumert, and G. J. Hurford, “The microwave brightness temperature spectrum of the quiet sun,” *Astrophys. J.* **370**, p. 779, 1991.
8. S. M. White, R. Thomas, J. W. Brosius, and M. R. Kundu, “The coronal abundance of Fe relative to H,” *Astrophys. J. (Lett.)* **534**, p. L203, 2000.
9. J. Zhang, M. R. Kundu, S. M. White, K. P. Dere, and J. S. Newmark, “Reconciling EUV and radio observations of the sun’s corona,” *Astrophys. J.* **561**, pp. 396–405, 2001.
10. S. Heddle and A. Webster, “Automation of imaging simulations for array configurations using classic AIPS,” *ALMA Memo Series* **290**, 2000.
11. J. Conway, “Self-similar spiral geometries for the LSA/MMA,” *ALMA Memo Series* **216**, 1998.
12. T. S. Bastian, D. E. Gary, S. M. White, and G. J. Hurford, “Broadband microwave imaging spectroscopy with a solar-dedicated array,” *Proc. SPIE* **3357**, p. 609, 1998.
13. B. G. Clark, “An efficient implementation of the CLEAN algorithm,” *A&A* **89**, p. 377, 1980.
14. T. J. Cornwell and K. F. Evans, “A simple maximum entropy deconvolution algorithm,” *Astron. Astrophys.* **143**, pp. 77–83, 1985.
15. R. D. Ekers and A. H. Rots, “Short Spacing Synthesis from a Primary Beam Scanned Interferometer,” in *IAU Colloq. 49: Image Formation from Coherence Functions in Astronomy*, C. van Schooneveld, ed., p. 61, D. Reidel, 1979.
16. T. J. Cornwell, “Radio-interferometric imaging of very large objects,” *A&A* **202**, pp. 316–321, 1988.
17. R. Sault, L. Staveley-Smith, and W. Brouw, “An approach to interferometric mosaicing,” *A&AS* **120**, p. 375, 1996.

18. T. J. Cornwell, M. A. Holdaway, and J. M. Uson, "Radio-interferometric imaging of very large objects: implications for array design," *A&A* **271**, p. 697, 1993.
19. J. E. Conway, T. J. Cornwell, and P. N. Wilkinson, "Multi-Frequency Synthesis - a New Technique in Radio Interferometric Imaging," *MNRAS* **246**, p. 490, 1990.
20. R. J. Sault and M. H. Wieringa, "Multi-frequency synthesis techniques in radio interferometric imaging.," *A&AS* **108**, pp. 585–594, 1994.